Supporting Information for:

Brownmillerite $Ca_2Co_2O_5$: Synthesis, Stability, and Re-entrant Single Crystal to Single Crystal Structural Transitions

Junjie Zhang,[*,†] Hong Zheng,[†] Christos D. Malliakas,[†] Jared M. Allred,[†] Yang Ren,[‡] Qing'an Li,[†] Tian-Heng Han[†,§] and J.F. Mitchell[†]

[†]Materials Science Division, Argonne National Laboratory, Argonne, Illinois 60439, United States

[‡]X-ray Science Division, Argonne National Laboratory, Argonne, Illinois, 60439, United States

[§]The James Franck Institute and Department of Physics, University of Chicago, Chicago, IL 60637, United States

Table S1. Atomic coordinates ($\times 10^4$) and equivalent isotropic displacement parameters ($Å^2 \times 10^3$) of $Ca_2Co_2O_5$ at various temperatures with estimated standard deviations in parentheses.

Table S2. Comparison of cobalt polyhedral distortion in $Ca_2Co_2O_5$, Ca_2FeCoO_5, $Ca_2Co_{1.54}Ga_{0.46}O_5$, and $Sr_2Co_2O_5$.

Table S3. Summary of space groups, interlayer separation, degree of twisting of the tetrahedral chains and the dipole moment of some brownmillerite oxides.

Table S4. Parameters from the final Rietveld refinement at each temperature for $Ca_2Co_2O_5$.

Fig. S1. Powder X-ray diffraction patterns of precursors.

Fig. S2. Comparison of the powder X-ray diffraction pattern of $Ca_2Co_2O_5$ and $Ca_2Co_{1.54}Ga_{0.46}O_5$.

Fig. S3. High pressure product at different pO_2.

Fig. S4. (a) High-resolution synchrotron X-ray pattern at 240 K with Rietveld fitting using *P*2/*c*11 single phase; (b) Zoom around 8.95º; (c) zoom around 6.42º.

Fig. S5. (a) High-resolution synchrotron X-ray pattern at 100 K with Rietveld fitting using *Pcmb* single phase; (b) Zoom around 8.95º; (c) zoom around 12.45º.

Fig. S6. (a) Isothermal field-dependent magnetization at 10 K for *H*//*b* following slow cooling (2 K/min from above room temperature to 260 K, 0.5 K/min from 260 to 90 K, then 2 K/min from 90 to 10 K) under 7 T and -7 T (M_{+7T} and $M_{-7\ T}$, respectively) showing vertical offset whose sign depends on that of the cooling field. (b) The function $(M_{+7T}-M_{-7T})/2$, which removes the offset observed in (a).

Table S1. Atomic coordinates ($\times 10^{-4}$) and equivalent isotropic displacement parameters ($Å^2 \times 10^{-3}$) of $Ca_2Co_2O_5$ from single crystal X-ray diffraction data at various temperatures.

Label	*x*	*y*	*z*	Occupancy	U_{eq}*	Label	*x*	*y*	*z*	Occupancy	U_{eq}*
300 K						**100 K**					
Ca(1)	-125(1)	1086(1)	7597(2)	1	10(1)	Ca(1)	-200(1)	1078(1)	2400(1)	1	5(1)
Ca(2)	4908(1)	3915(1)	4904(2)	1	10(1)	Ca(2)	4892(1)	3922(1)	5099(1)	1	6(1)
Co(1)	4509(1)	2500	7200(1)	1	9(1)	Co(1)	4462(1)	2500	2804(1)	1	5(1)
Co(2)	-458(1)	2500	5298(1)	1	9(1)	Co(2)	-468(1)	2500	4702(1)	1	5(1)
Co(3)	0	0	5000	1	7(1)	Co(3)	0	0	5000	1	4(1)
Co(4)	-5047(1)	0	7500	1	7(1)	Co(4)	-5107(1)	0	2500	1	3(1)
O(1)	896(4)	2500	6927(2)	1	11(1)	O(1)	879(4)	2500	3084(2)	1	6(1)
O(2)	5928(4)	2500	5576(2)	1	11(1)	O(2)	5954(4)	2500	4400(2)	1	6(1)
O(3)	190(3)	3602(3)	4704(5)	1	13(1)	O(3)	223(3)	3608(2)	5307(3)	1	9(1)
O(4)	5088(3)	1396(3)	7796(5)	1	15(1)	O(4)	5045(3)	1386(2)	2198(3)	1	9(1)
O(5)	-2440(4)	-99(2)	3742(5)	1	11(1)	O(5)	-2367(3)	-102(2)	6257(2)	1	6(1)
O(6)	-2566(4)	140(2)	6241(5)	1	10(1)	O(6)	-2631(3)	150(2)	3762(2)	1	6(1)
240 K						**200 K**					
Ca(1)	9808(2)	6074(1)	7405(2)	1	9(1)	Ca(1)	205(2)	1079(1)	2604(1)	1	8(1)
Ca(2)	148(2)	1082(1)	2603(2)	1	9(1)	Ca(2)	202(2)	6078(1)	2405(1)	1	8(1)
Ca(3)	4903(2)	1081(1)	4905(2)	1	9(1)	Ca(3)	4900(2)	6081(1)	102(1)	1	8(1)
Ca(4)	5095(2)	6077(1)	5102(2)	1	9(1)	Ca(4)	4898(2)	1078(1)	4904(1)	1	8(1)
Co(1)	5525(1)	2512(1)	2193(1)	1	8(1)	Co(1)	4454(2)	2500	7191(1)	1	7(1)
Co(2)	466(1)	2494(1)	300(1)	1	8(1)	Co(2)	5548(2)	2500	2195(1)	1	8(1)
Co(3)	0	0	0	1	6(1)	Co(3)	462(2)	2500	297(1)	1	8(1)
Co(4)	0	5000	0	1	7(1)	Co(4)	9528(2)	2500	5299(1)	1	7(1)
Co(5)	5067(1)	0	2500	1	6(1)	Co(5)	0	0	5000	1	6(1)
Co(6)	4898(2)	5000	7500	1	5(1)	Co(6)	0	0	0	1	6(1)
						Co(7)	5112(1)	1(1)	2503(1)	1	6(1)
O(1)	4061(5)	2506(2)	590(3)	1	10(1)	O(1)	878(5)	2500	6924(3)	1	8(1)
O(2)	-877(4)	2500(2)	1923(2)	1	9(1)	O(2)	9132(5)	2500	1927(3)	1	9(1)
O(3)	4924(4)	1417(3)	2800(4)	1	12(1)	O(3)	5942(5)	2500	5597(3)	1	8(1)
O(4)	4978(4)	3644(3)	2780(4)	1	13(1)	O(4)	4056(5)	2500	593(3)	1	9(1)
O(5)	-228(5)	3589(3)	-310(4)	1	13(1)	O(5)	217(5)	1394(2)	4703(3)	1	12(1)
O(6)	2384(5)	5097(2)	-1259(3)	1	9(1)	O(6)	234(5)	6402(2)	308(3)	1	11(1)
O(7)	7370(5)	5143(2)	8755(3)	1	9(1)	O(7)	4971(5)	6382(2)	2206(3)	1	12(1)
O(8)	2417(5)	-102(2)	-1258(3)	1	9(1)	O(8)	4963(5)	1386(2)	2806(3)	1	13(1)
O(9)	2584(5)	146(2)	1244(3)	1	9(1)	O(9)	2382(4)	98(2)	6263(3)	1	9(1)
O(10)	-189(5)	1373(3)	-293(4)	1	12(1)	O(10)	7639(4)	103(2)	1255(3)	1	9(1)
						O(11)	2620(4)	5146(2)	3765(3)	1	9(1)
						O(12)	2664(4)	149(2)	1255(3)	1	8(1)

*U_{eq} is defined as one third of the trace of the orthogonalized U_{ij} tensor.

Table S2. Comparison of cobalt polyhedral distortion in $Ca_2Co_2O_5$, Ca_2FeCoO_5, $Ca_2Co_{1.54}Ga_{0.46}O_5$, and $Sr_2Co_2O_5$.

Compound	Temperature (K)	Tetrahedral distortion ($\times10^{-4}$)	Octahedral distortion ($\times10^{-4}$)
$Ca_2Co_2O_5$	300	12.7, 11.9 (average: 12.3)	23.5, 22.4 (average: 23.0)
	240	11.7, 10.5 (average: 11.1)	13.6, 25.7, 24.9, 8.6 (average: 18.2)
	200	9.4, 10.2, 13.7, 11.5 (average: 11.2)	19.4, 22.8, 15.1 (average: 19.1)
	100	11.1, 10.3 (average: 10.7)	19.6, 13.1 (average: 16.4)
Ca_2FeCoO_5[S1]	300	8.2	13.4
$Ca_2Co_{1.54}Ga_{0.46}O_5$[S2]	300	6.9	30.6
$Sr_2Co_2O_5$[S3]	300	11.9	45.8
	200	5.7	45.6
	100	3.5	44.0

Table S3 Summary of space groups, interlayer separation (*b*/2), degree of twisting of the tetrahedral chains (O-O-O angle) and dipole moment for some brownmillerite oxides.

Compound	Space group[a]	b/2 (Å)	O-O-O angle (°)	Dipole moment of each tetrahedral (Debye)	Net dipole moment along each chain		Tetrahedral site
					$\times10^{-4}$ esu·cm/Å^3	Debye	
Ca_2FeAlO_5[S4]	*I*2*mb*	7.25	131.5	FeO_4: 2.45; AlO_4: 2.61	16.8	1.4	Disorder
Ca_2FeGaO_5[S5]	*Pnma*	7.35	125.8	GaO_4: 1.70	17.7	1.6	Order
$Ca_2Fe_{1.66}V_{0.34}O_5$[S6]	*Pnma*	7.37	125.8	FeO_4: 2.46	20.2	1.8	Order
$Ca_2Fe_2O_5$[S7]	*Pnma*	7.41	125.3	FeO_4: 2.16	21.4	1.9	Order
Ca_2FeCoO_5[S1]	*Pcmb*	7.41	123.5	CoO_4: 2.56; FeO_4: 3.00	33.8	3.0	Order
$Ca_2Co_{1.54}Ga_{0.46}O_5$[S2]	*Pnma*	7.44	123.7	CoO_4: 2.60; GaO_4: 2.58	40.4	3.5	Disorder
$Ca_2Co_2O_5$	*Pcmb*	7.46	121.5	CoO_4: 3.35, 3.33	45.2	3.9	Order
$SrCaMnGaO_5$[S8]	*I*2*mb*	7.89	124.2	GaO_4: 3.39	35.0	3.2	Order
$LaCaCuGaO_5$[S9]	*I*2*mb*	7.92	124.5	GaO4: 2.21	22.5	2.1	Order
$La_{1.2}Sr_{0.8}Mn_2O_5$[S10]	*Pcmb*	8.31	111.8	MnO_4: 5.20, 5.01	63.4	6.3	Order

Calculation Details

A bond-valence approach has been used to calculate the direction and magnitude of the dipole moments for each tetrahedron. The local dipole moment of a tetrahedron can be calculated using the Debye equation, $\mu=neR$ (μ is the net dipole moment in Debye, n is the total number of electrons, e is the charge on an electron, and R is the distance in cm between the "centroids" of positive and negative charge).[S11,S12] The distribution of electrons on each atom was estimated using bond valence theory.[S13,S14] To calculate the net dipole moment along each chain, we normalized the unit cell to dimensions ~5×11×15 Å^3. For Ca_2FeAlO_5 and $Ca_2Co_{1.54}Ga_{0.46}O_5$ with disordered atoms in tetrahedral sites, the net dipole moment along each chain was calculated by taking into account the statistical occupancy.

Table S4. Parameters from the final Rietveld refinement at 300, 240, 200 and 100 K for $Ca_2Co_2O_5$.

T (K)	Space Group	Phase (wt%)	Lattice parameters					Quality of Fit		
			a (Å)	*b* (Å)	*c* (Å)	*β* (°)	V (Å^3)	R_{wp}	R_p	χ^2
300	***Pcmb***	100	5.288203(13)	14.924582(38)	10.953042(23)	-	864.460(2)	13.46%	10.91%	2.262
240	***Pcmb***	20	5.291507 (100)	14.851301 (247)	10.962284 (117)	-	861.479(18)	12.87%	9.55%	2.938
	P2/c11	80	5.292553 (27)	14.807267 (89)	10.964293(34)	90.158	859.249(6)			
200	***P12$_1$/m1***	100	5.299726(15)	14.781377 (45)	10.976010(22)	90.329	859.816(3)	12.22%	9.03%	2.874
100	***P12$_1$/m1***	8	5.299893(62)	14.750240(240)	10.982167(146)	90.406	858.506(15)	14.14%	10.25%	4.210
	Pcmb	92	5.302917(11)	14.749347(35)	10.986770(22)	-	859.325(2)			

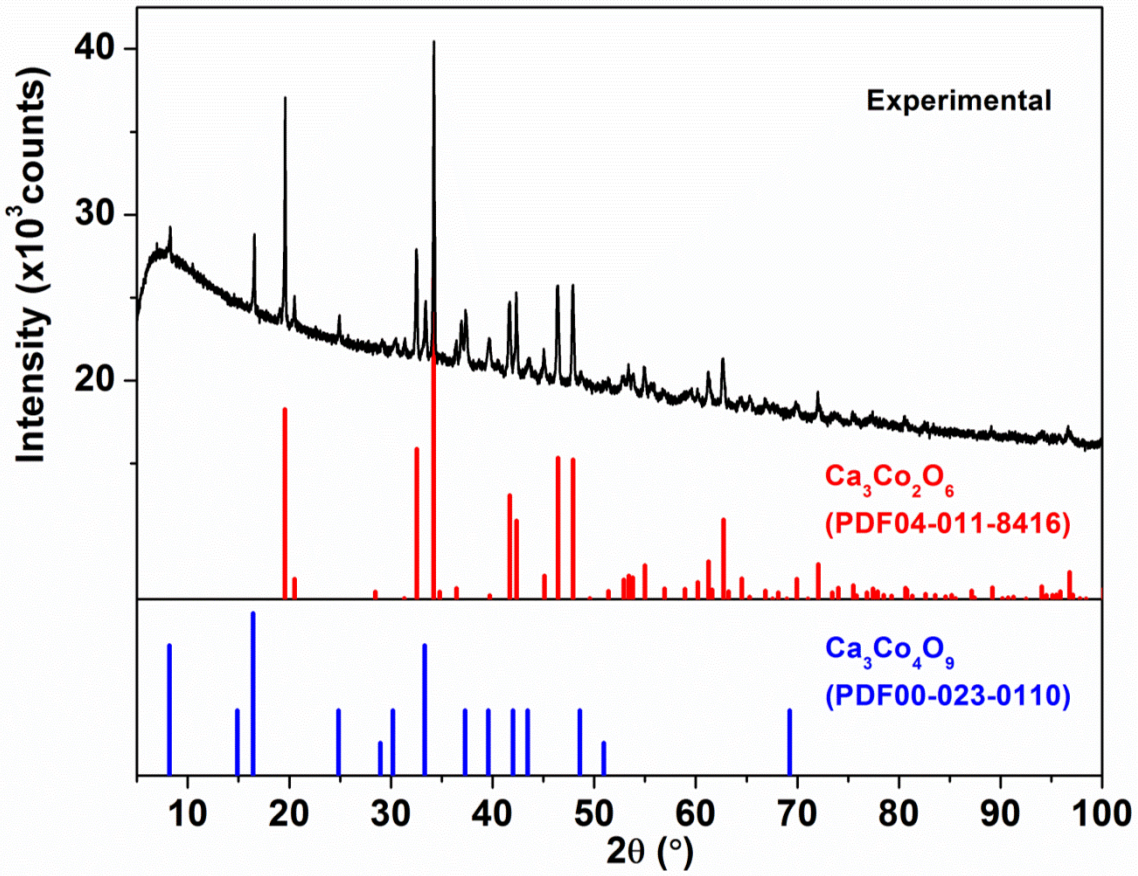

Fig. S1. Powder X-ray diffraction patterns of precursors.

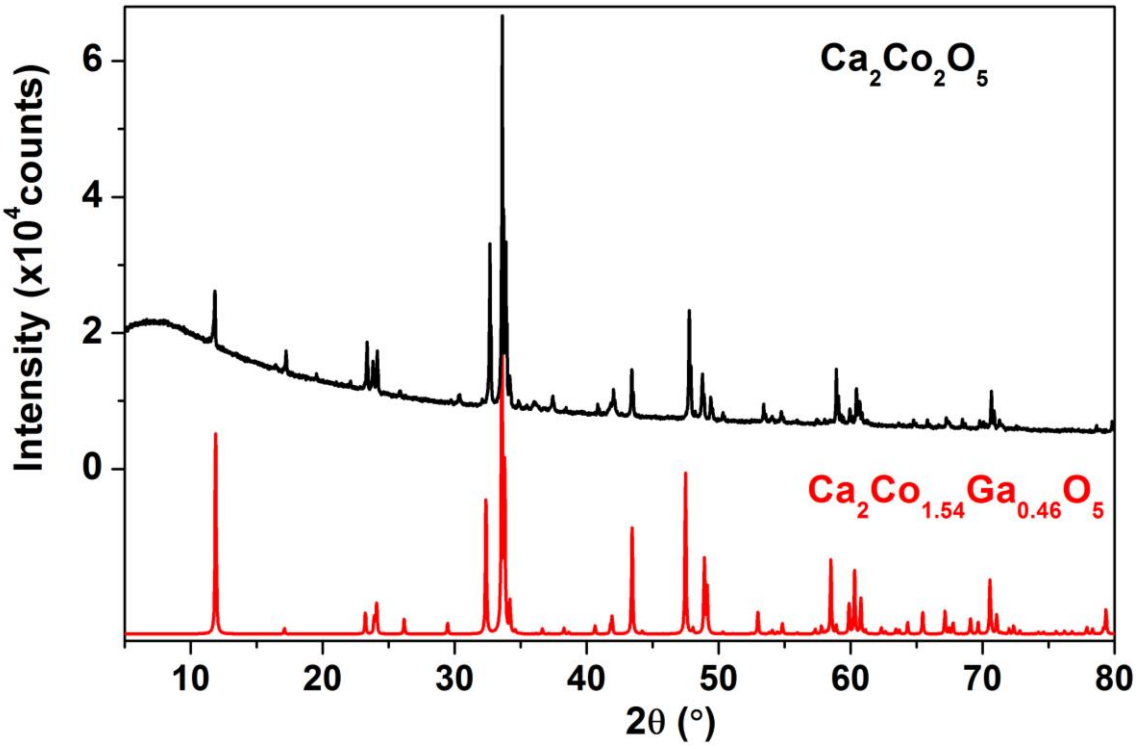

Fig. S2. Comparison of the powder X-ray diffraction pattern of $Ca_2Co_2O_5$ and $Ca_2Co_{1.54}Ga_{0.46}O_5$. The latter pattern is calculated from the single crystal structure in Ref. S2.

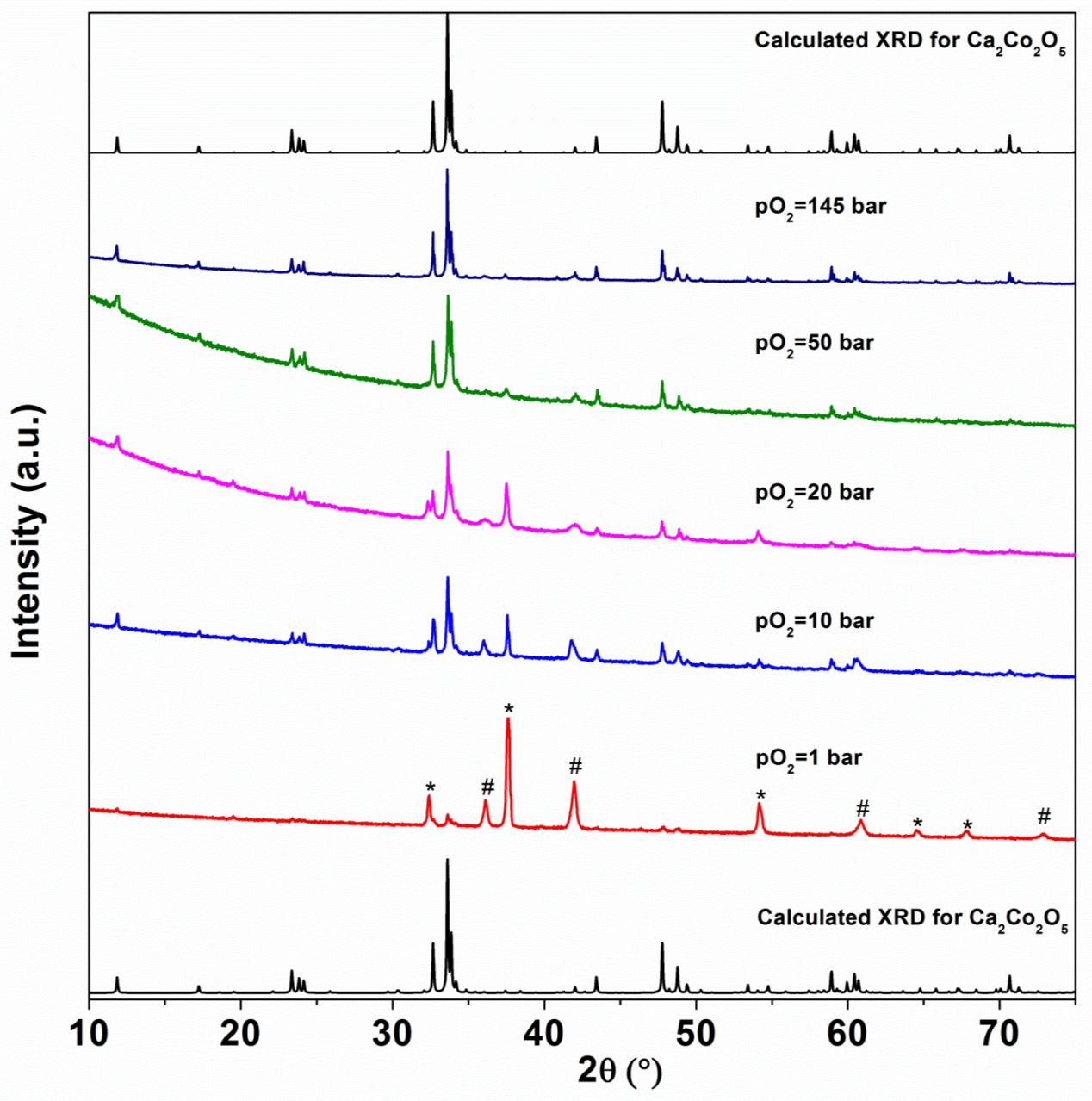

Fig. S3. Synthesis products as a function of pO_2. Note CaO (*) and CoO (#).

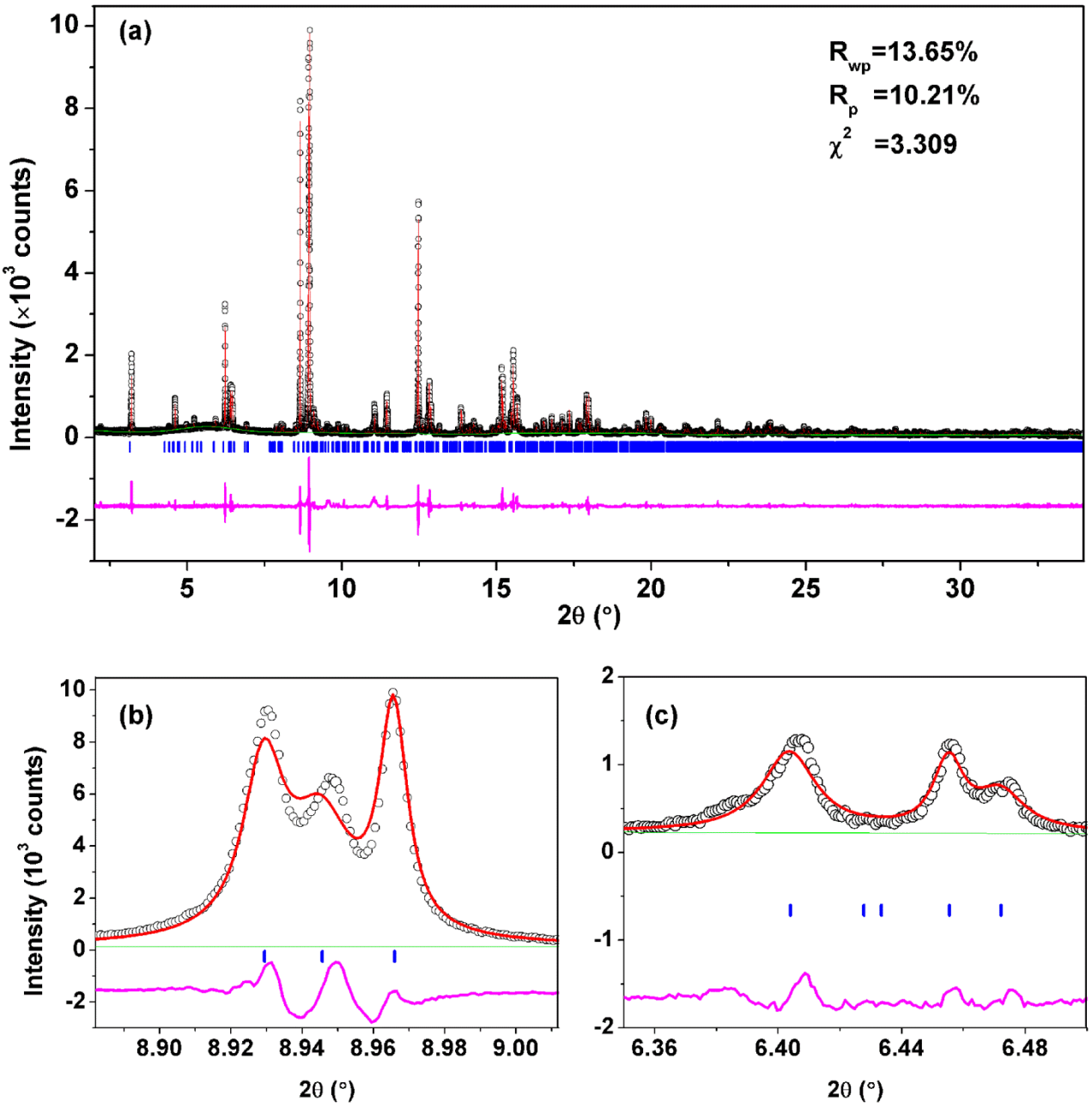

Fig. S4. (*a*) High-resolution synchrotron X-ray pattern at 240 K with Rietveld fitting using a single *P*2/*c*11 phase; (*b*) detail around 8.95º; (*c*) detail around 6.42º. The black circle, red line, green line, blue bars and magenta line correspond to the observed data, calculated intensity, background, Bragg peaks, and difference curve, respectively. Compared to the two-phase (*P*2/*c*11+ *Pcmb*) refinement in Fig. 5(*b*) of the main text, the fit is markedly worse.

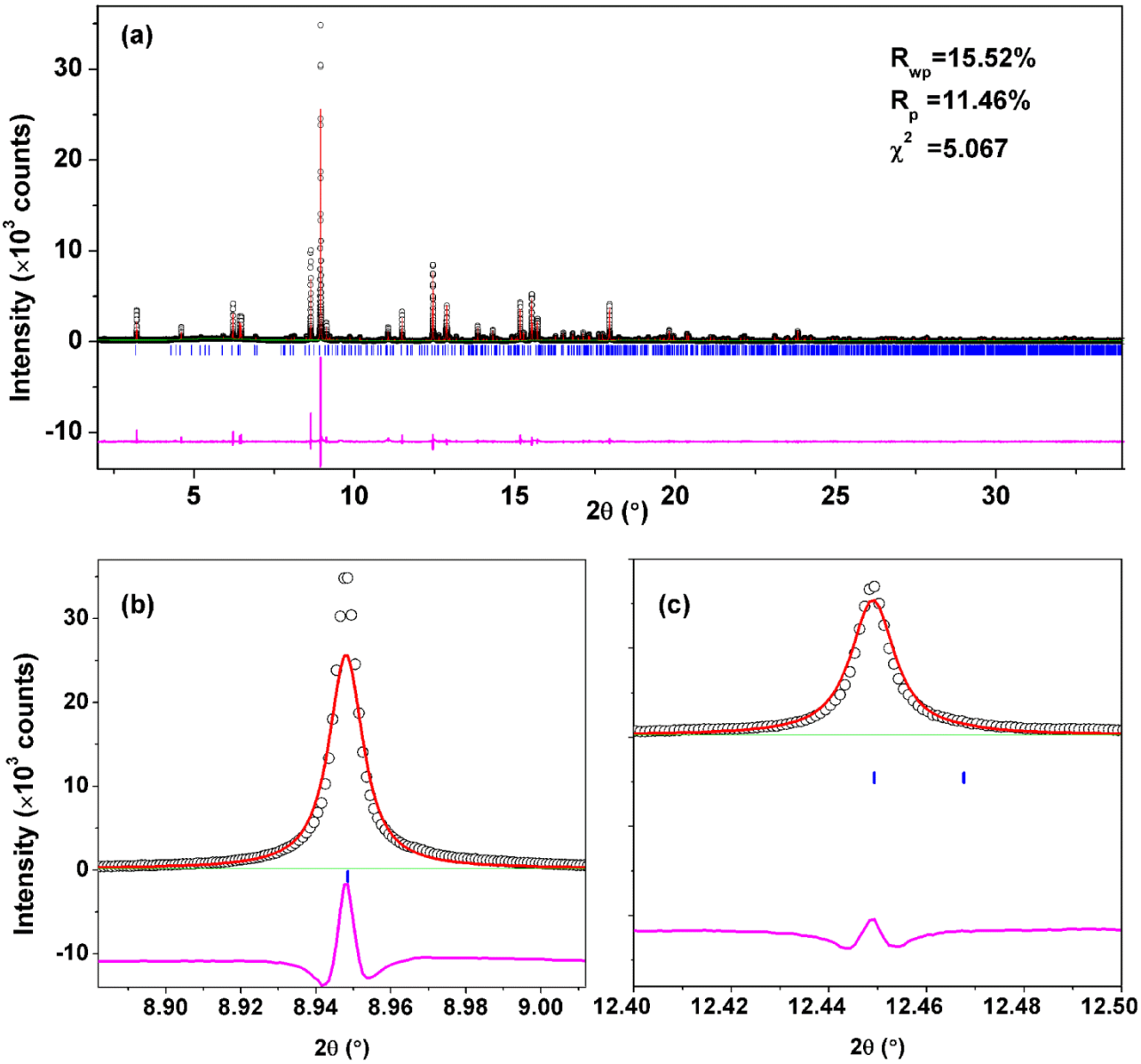

Fig. S5. (*a*) High-resolution synchrotron X-ray pattern at 100 K with Rietveld fitting using *Pcmb* single phase; (*b*) detail around 8.95º; (*c*) detail around 12.45º. The black circle, red line, green line, blue bars and magenta line correspond to the observed data, calculated intensity, background, Bragg peaks, and difference curve, respectively. Compared to the two-phase ($P12_1/m1$+ *Pcmb*) refinement in Fig. 5(*d*) of the main text, this fit is markedly worse.

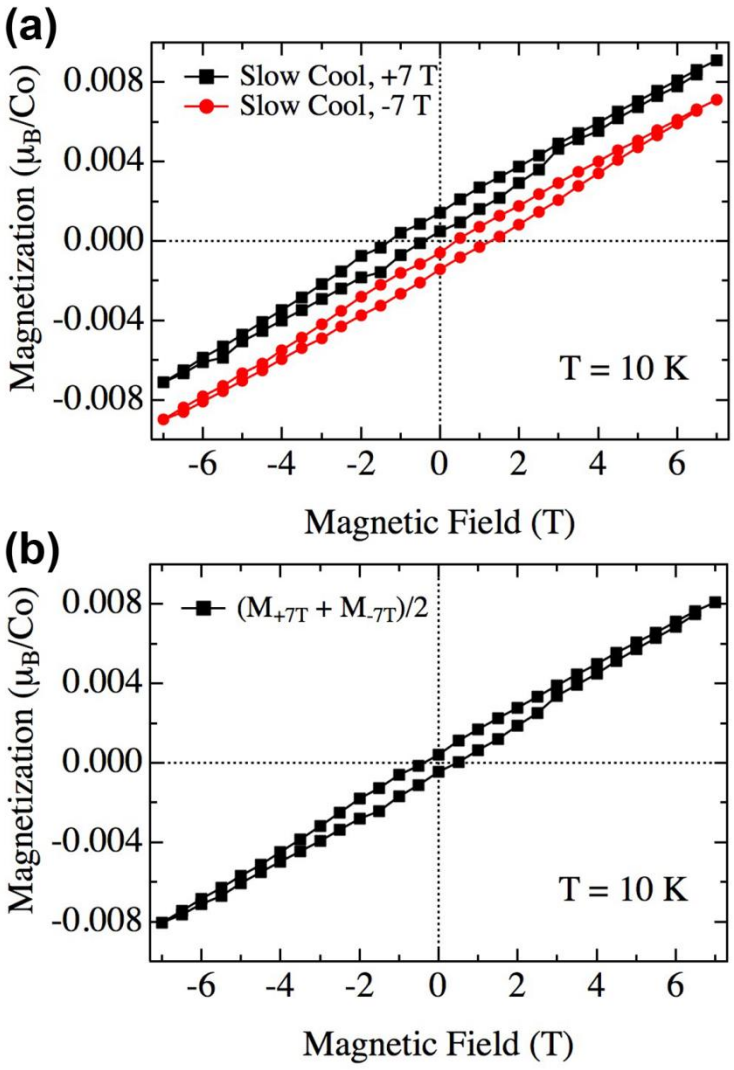

Fig. S6. (*a*) Isothermal field-dependent magnetization at 10 K for *H*//*b* following slow cooling (2 K/min from above room temperature to 260 K, 0.5 K/min from 260 to 90 K, then 2 K/min from 90 to 10 K) under 7 T and -7 T (M_{+7T} and $M_{-7\,T}$, respectively) showing vertical offset whose sign depends on that of the cooling field. (*b*) The function $(M_{+7T}-M_{-7T})/2$, which removes the offset observed in (*a*).

Fig. S6 shows the isothermal field-dependent magnetization along the *b*-axis following slow cooling (2 K/min from above room temperature to 260 K, 0.5 K/min from 260 to 90 K, and 2 K/min from 90 to 10 K) to 10 K in either +7 T or -7 T. A small vertical offset of the data is observed in either case, with opposite sign. We conclude that this small offset (not observed in the ZFC data, see **Fig. 7** of main text) arises from a component in the sample that becomes magnetized during the field-cooling process. The nature of this extremely small ferromagnetic component is not known. However, the data of **Fig. S6(*a*)** demonstrate that it cannot be reversed by application of fields as high as 7 T. The small data offset (amounting to ~0.001 μ_B/Co) can be subtracted by computing $(M_{+7T}-M_{-7T})/2$, with the result shown in **Fig. S6(*b*)**, the same data plotted in Fig 7(d) of the main text. The remanent moment of ~0.0004 μ_B/Co represents either the upper bound on the ordered moment of $Ca_2Co_2O_5$ under these conditions (almost three orders of magnitude less than that found for the fast cooling protocol (**Fig. 7(*b*)** main text) or a signal arising from some other unidentified weakly ferromagnetic impurity phase.

References

(S1)Ramezanipour, F.; Greedan, J. E.; Grosvenor, A. P.; Britten, J. F.; Cranswick, L. M. D.; Garlea, V. O. *Chem. Mater.* **2010**, *22*, 6008.

(S2)Istomin, S. Y.; Abdyusheva, S. V.; Svensson, G.; Antipov, E. V. *J. Solid State Chem.* **2004**, *177*, 4251.

(S3)Sullivan, E.; Hadermann, J.; Greaves, C. *J. Solid State Chem.* **2011**, *184*, 649.

(S4)Jupe, A. C.; Cockcroft, J. K.; Barnes, P.; Colston, S. L.; Sankar, G.; Hall, C. *J. Appl. Crystallogr.* **2001**, *34*, 55.

(S5)Arpe, R.; Müller-Buschbaum, H.; Schenck, R. V. *Z. Anorg. Allg. Chem.* **1974**, *410*, 97.

(S6)Harringer, N. A.; Presslinger, H.; Klepp, K. O. *Z. Kristallogr. - New Cryst. Struct.* **2004**, *219*, 5.

(S7)Berastegui, P.; Eriksson, S. G.; Hull, S. *Mater. Res. Bull.* **1999**, *34*, 303.

(S8)Battle, P. D.; Bell, A. M. T.; Blundell, S. J.; Coldea, A. I.; Gallon, D. J.; Pratt, F. L.; Rosseinsky, M. J.; Steer, C. A. *J. Solid State Chem.* **2002**, *167*, 188.

(S9)Luzikova, A. V.; Kharlanov, A. L.; Antipov, E. V.; Müller-Buschbaum, H. *Z. Anorg. Allg. Chem.* **1994**, *620*, 326.

(S10) Parsons, T. G.; D'Hondt, H.; Hadermann, J.; Hayward, M. A. *Chem. Mater.* **2009**, *21*, 5527.

(S11) Maggard, P. A.; Nault, T. S.; Stern, C. L.; Poeppelmeier, K. R. *J. Solid State Chem.* **2003**, *175*, 27.

(S12) Zhang, J.; Zhang, Z.; Zhang, W.; Zheng, Q.; Sun, Y.; Zhang, C.; Tao, X. *Chem. Mater.* **2011**, *23*, 3752.

(S13) Brown, I. D.; Altermatt, D. *Acta Crystallogr. Sect. B: Struct. Sci.* **1985**, *41*, 244.

(S14) Brese, N. E.; O'Keeffe, M. *Acta Crystallogr. Sect. B: Struct. Sci.* **1991**, *47*, 192.